Astrophys. Bulletin, 2007, 62, 285-295 © Pleiades Publishing, Ltd. SPRINGER 2008

On the Antenna Beam Shape Reconstruction Using Planet Transit

P.D. Naselsky[a], O.V. Verkhodanov[b], P.R. Christensen[a], L.-Y. Chiang[a]

[a] Niels Bohr Institute, Blegdamsvej 17, DK-2100 Copenhagen, Denmark
[b] Special Astrophysical Observatory of the Russian AS, Nizhnij Arkhyz 369167, Russia

Received December 18, 2006; accepted January 17, 2007.

arXiv:astro-ph/0211093v3 27 Dec 2007

The calibration of the in-flight antenna beam shape and possible beam degradation is one of the most crucial tasks for the upcoming Planck mission. We examine several effects which could significantly influence the in-flight main beam calibration using planet transit: the problems of the variability of the Jupiter's flux, the antenna temperature and passing of the planets through the main beam. We estimate these effects on the antenna beam shape calibration and calculate the limits on the main beam and far sidelobe measurements, using observations of Jupiter and Saturn. We also discuss possible effects of degradation of the mirror surfaces and specify corresponding parameters which can help us to determine these effects.

1. INTRODUCTION

The ESA Planck Surveyor [1] is designed to image the whole sky of the Cosmic Microwave Background (CMB) radiation with unprecedented sensitivity ($\Delta T/T \sim 2 \times 10^{-6}$) and angular resolution (down to $5'$) at 9 frequencies: 30, 44, 70, 100, 143, 217, 353, 545, 857 GHz at Low Frequency Instrument (LFI) [1] and High Frequency Instrument (HFI) [2].

To achieve these high sensitivity and resolution, it is necessary to carefully account for all potential systematic features in the data [3].

One of the systematic effects is related to the in-flight antenna beam shape and its reconstruction. Apart from the need to acquire the radiation pattern of the antenna beam before the flight, the calibration of the in-flight antenna beam shape is one of the key components for achieving the scientific goals of the Planck mission. This problem has been considered by different Planck groups [4, 5, 6, 7], and recently by [8, 9].

The accuracy of the CMB anisotropy C_ℓ estimation will be affected, among other experiment parameters, by our ignorance of the in-flight antenna beam shape of the main beam and far sidelobes, and possible degradation of the mirror surface shapes. When scanning the antenna beam of the Planck mission is to move across the sky, implying that the antenna beam response is a function of time. After pixelization of the time-ordered data the position of each pixel on the pixelized CMB map is directly related to some data points in the time stream. It is therefore necessary to obtain the information about the in-flight beam shape, its inclination and the location of the beam center relative to each pixel, in order to improve the model of the in-flight main beam shape as well as in the far sidelobe region.

To tackle this issue, Burigana et al. [6] have suggested a method which uses planet transit to reconstruct the in-flight beam shape. These planet crossings can help the in-flight beam recovery down to $-25 \div 32.5$ dB at 30 GHz. They also showed that the main beam pattern can be described by the bivariate Gaussian approximation. Recently Chiang et al. [7] have proposed another method for the beam shape estimation based on the interplay of amplitudes and phases of the sky signal and instrumental noise. This method is useful in extraction of the antenna main beam shape down to $-7 \div 10$ dB, and does not need a strong radio source shape calibration. These methods have laid a base for the determination of both the in-flight antenna beam shape and its variations during observations.

The aim of this paper is to re-examine in details the proposed method of the in-flight antenna shape reconstruction by planet crossing [6] in order to estimate possible beam degradation effects. The method, based on Jupiter and Saturn observations, has some subtleties needed to be addressed such as the temporal and frequency variations of the Jupiter's flux and

[1] `http://astro.estec.esa.nl/SA-general/Projects/Planck/`

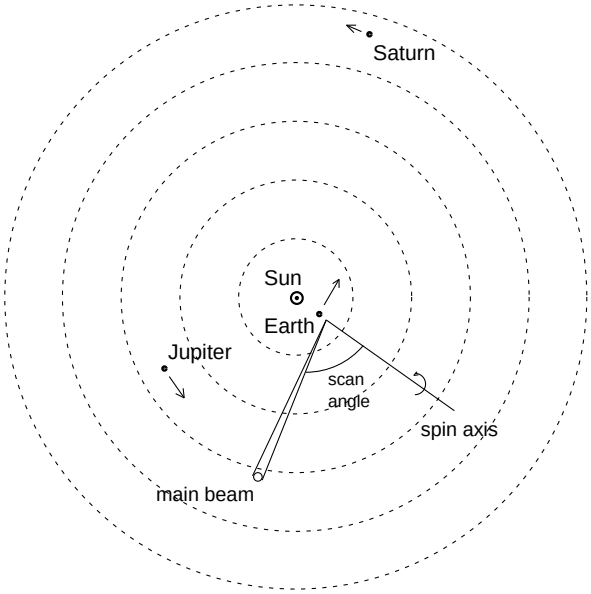

Figure 1: *Positions of Jupiter and Saturn at the beginning of the Planck mission (November, 2008). The radius of each concentric circle is differed by 2 AU.*

passing of the planets through the main beam.

This paper is arranged as follows. In Section 2 we describe the Planck scan strategy in relation to planet observations, and the beam definitions. In Section 3 we discuss the in-flight beam calibration using planet transit. We concentrate in Section 4 on the effects in beam calibration due to fluctuation of the Jupiter's flux density. In Section 5 we discuss variations arising from the distance to the planets and from the scan strategy. Conclusion is in Section 6.

2. SCAN STRATEGY AND THE BEAM PROBLEM

The proposed scan strategy [4] for the Planck mission is a whole-sky scanning with the satellite orbiting around the L2 Lagrangian point of the Earth–Sun system. The satellite spin axis will be pointed in the anti-Sun direction and will have a tilt to the ecliptic plane of 10°. The telescope optical angle is inclined at 85° to the spin axis. The telescope will scan the same circle 60 times around the spin axis at 1 r.p.m. Each hour the spin axis will be shifted along the ecliptic plane with a step of 2′.5 during the entire mission (about 15 months).

2.1. Observations of the Planets

According to the present schedule, the launch of the satellite is planned in June 30, 2008 and the flight to the L2 point will take approximately six months. To construct the L2, Earth, Jupiter and Saturn orbiting around the Sun, we use the planets ephemerides calculation procedure of the XEphem.3.7.2 software by [10] (see Fig. 1).

As mentioned above, the scan angle is assigned to be 85°. Assuming the beginning of the mission on the 31th of October 2008, in 15 months Jupiter will cross the main beam direction 3 times on the dates of 22.05.2009, 03.11.2009 and 27.01.2010 (and on 09.12.2010) with an accuracy of ±1.5 day, mainly due to tilt and starting conditions, whereas Saturn will cross the main beam 3 times on the dates of 17.12.2008, 31.05.2008 and 30.12.2009 (and in 2010, on 11.06.2010) (Fig. 2).

As shown in Fig. 2, the antenna beam shape calibrations using Jupiter and Saturn can only be realized 6 (3 + 3) times during the mission with a few different time intervals between each planet crossing. These "windows" provide us with the possibility of estimating degradation of the antenna main beam shape from the long time frequencies (up to 15 months) to the short frequencies (about 10 days).[2] For continuous calibration of the main beam area, therefore, it is necessary to use the method by [7] to reconstruct its ellipticity and orientation in the data analysis. One of the interesting dates in the planet observation is 03.11.2009, when Jupiter and Mars could be observed during one day. Unfortunately, the unpredictability of the Mars spectrum in the millimeter wavelength range due to atmosphere storms [11] does not allow us to calibrate the far sidelobes. However, the mission can provide interesting results for the study of Mars [22].

2.2. Inclination of the Planet Orbits to the Ecliptic Plane

We make our estimation of the planet transit for the ecliptic plane projection. However, the planets have ecliptic latitude different from zero. The maximum inclinations are ≈ 1° for Jupiter and ≈ 2° for Saturn (the detailed calculation for each planet crossing is in Table 1). Here we note that this problem is not essential for our case but is similar to the tilt projection problem discussed below.

According to the scan strategy proposals the spin axis can have a tilt to the ecliptic plane of about 10°. This means that the usual ecliptic projection of the scan angle will be narrower and we shall observe

[2] The interesting point of the track crossing between Jupiter and Saturn near the scan angle on 26.05.2009 allows us to discuss the possibility of simultaneous observations of two planets in one scan. However, to make such observations, we need to have a scan angle of about 80°. Otherwise, these transits can be used to test the far sidelobes of the beam.

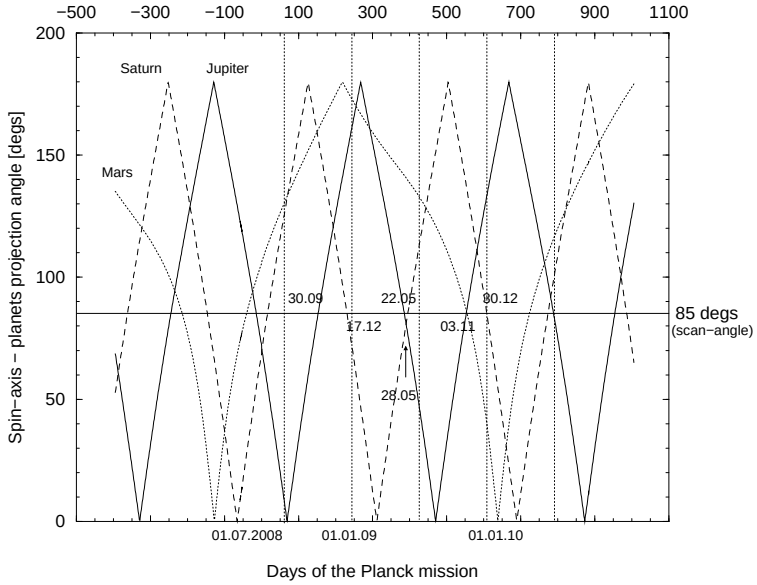

Figure 2: *Transit of Saturn, Jupiter and Mars through a scan angle of* 85°. *The dashed, solid and dotted curves represent the Saturn, Jupiter and Mars paths, respectively. The solid horizontal line demonstrates a scan angle of 85°. Dates near the horizontal line correspond to the Jupiter's and Saturn's crossings of the 85° scan angle.*

Table 1: *Position of the planets on the dates of crossing by Planck on the ecliptic plane and antenna temperatures ($T_a = \Omega_{\rm planet}/\Omega_{\rm beam} \cdot T_b$) in transit via scan angle of 85°*

Planet	Date 85°	Size (arcsec)	T_a (mK) 30 GHz 33′	100 GHz 10′	545 GHz 5′	Ecliptic latitude	Ecliptic longitude
Saturn	17.12.2008	17.9	7.534	86.98	291.2	+1:58.0	171:27.2
Jupiter	22.05.2009	40.4	43.86	556.3	1672	−0:45.6	325:59.8
Saturn	31.05.2009	17.9	7.534	86.98	291.2	+2:07.8	164:57.5
Jupiter	03.11.2009	40.9	44.40	563.2	1693	−1:01.2	317:46.9
Saturn	30.12.2009	17.7	7.450	86.01	287.9	+2:16.9	184:19.6
Saturn	17.06.2010	17.5	7.366	85.04	284.7	+2:21.9	177:57.1
Jupiter	27.06.2010	40.4	43.86	556.3	1672	−1:16:03	2:10:53

Jupiter on other days with another antenna temperature. The scan projection ψ of the scan angle α for the tilt angle ϕ can be calculated as

$$\tan\psi = \tan\phi\cos\alpha, \qquad (1)$$

which gives us $\psi = 84.92°$, for $\alpha = 85°$ and $\phi = 10°$. This difference is within $5'$, indicating that the projections of the planet trajectories and the tilt of the axis will not interfere with our estimates.

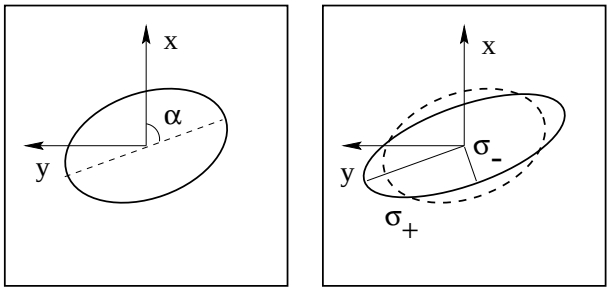

Figure 3: *Beam degradation parameters. The left panel illustrates the orientation angle of the beam, and the right panel shows σ_- and σ_+, the semi-minor and semi-major axes of the elliptical main beam.*

2.3. Beam Descriptions and its Variations Due to Mirror Degradation

The Planck "antenna beam" is usually referred to as a physical model of the antenna response and its ground-based verification before the flight, and the *in-flight* antenna beam as the beam reconstructed during

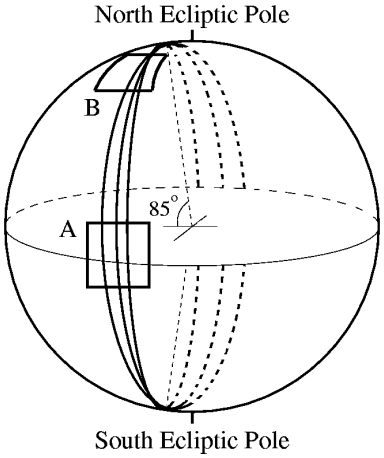

Figure 4: *The Planck scan strategy. The square A is located at the parallel scan area, where the planets can be found. The square B has crossing(s) of the circular scans.*

the flight, which is crucial for possible beam degradation estimation. The in-flight antenna beam plays a significant role in the C_ℓ estimation as well as in the extra-galactic point source extraction [12].

Physics optics calculations have shown that the main beam is roughly elliptical [13, 6], so we can approximate the antenna pattern as a bivariate Gaussian beam. The geometrical property of the beam in the time domain can be described as follows. We denote by x_0 and y_0 the position of the beam in a coordinate system fixed to the detector with x in scan direction and y perpendicular to x and the beam axis. Then the beam shape can be written as

$$B_t(\vec{x}-\vec{x}_t) = \exp\left[-\frac{1}{2}(\mathsf{RU})^{\mathrm{T}}\mathsf{D}^{-1}(\mathsf{RU})\right], \quad (2)$$

with

$$\mathsf{U} = \begin{pmatrix} x-x_0 \\ y-y_0 \end{pmatrix}, \quad (3)$$

where R is the rotation matrix which describes the inclination of the elliptical beam,

$$\mathsf{R} = \begin{pmatrix} \cos\alpha & \sin\alpha \\ -\sin\alpha & \cos\alpha \end{pmatrix}, \quad (4)$$

with α being the orientation angle between the x axis and the major axis of the ellipse. The D matrix denotes the beam width along the ellipse major axis, which can be expressed as

$$\mathsf{D} = \begin{pmatrix} \sigma_+^2 & 0 \\ 0 & \sigma_-^2 \end{pmatrix}. \quad (5)$$

If, during the routine operation, the mirror surfaces are slightly perturbed (deformed), it is necessary to conduct a detailed investigation of the corresponding degradation of the antenna beam shapes, using Jupiter's and Saturn's transits as suggested by [6][3]. In general, beam degradation can be described by 3 parameters as illustrated in Fig. 3. First of all, the mean beam width is a function of time,

$$\frac{1}{2}(\sigma_-^2+\sigma_+^2) \equiv \sigma^2 = \sigma^2(t), \quad (6)$$

where σ_- and σ_+ are the minor and major axes of the elliptical main beam. The orientation angle α between the scan direction and the major axis of the elliptical main beam can also be a function of time, i.e.,

$$\alpha \equiv \alpha(t). \quad (7)$$

and so can the ellipticity ratio of the beam

$$\frac{\sigma_+}{\sigma_-} = \rho \equiv \rho(t). \quad (8)$$

We can use these 3 parameters as the indicators of the degradation level of the in-flight antenna beam.

3. PLANET TRANSITS AND THE PIXEL DOMAIN

Following [6], we can specify the in-flight Planck antenna beam shape model by using Jupiter as a "standard candle" for calibration. For the Planck (both LFI and HFI) frequency ranges we can model the Jupiter's contribution to the resulting $\Delta T(\boldsymbol{r})$ sky temperature in some direction $\boldsymbol{r}$ as

$$\Delta T_{\mathrm{J}}(\boldsymbol{r}) = \frac{S_{\mathrm{J}}(\nu,t)}{2k}\left(\frac{hc}{kT_{\mathrm{CMB}}}\right)^2\left[\frac{2\sinh(\eta/2)}{\eta^2}\right]^2\delta(\boldsymbol{r}_{\mathrm{J}},\boldsymbol{r}), \quad (9)$$

where $\boldsymbol{r}$ and $\boldsymbol{r}_{\mathrm{J}}$ are the unit vectors in the corresponding direction on the sky and Jupiter's location in a given coordinate system, respectively, $\delta(\boldsymbol{r}_{\mathrm{J}},\boldsymbol{r})$ is the Dirac delta function, S_{J} is the Jupiter's flux, T_{CMB}, h, k and c are the CMB temperature, Planck constant, Boltzmann constant, and speed of light, respectively, and $\eta = h\nu/kT_{\mathrm{CMB}}$.

Each observed time-ordered subscan m_t^i that includes Jupiter's image is related to $\Delta T_{\mathrm{J}}(\boldsymbol{r})$ from Eq. (9) through a convolution with the antenna beam function $B(\boldsymbol{r},\boldsymbol{r}')$ (see [7])

$$y_t^i = d_t^i + n_t^i, \quad (10)$$

where

$$d_t^i = \Delta T_{\mathrm{J}}[\boldsymbol{r}(t)] \otimes B[\boldsymbol{r}(t^i),\vec{r}(t)], \quad (11)$$

where $\otimes$ denotes convolution, and n_t^i now is the CMB signal plus all the foregrounds and the instrumental

[3] As we will see in the next section, the Jupiter's flux fluctuation could mimic the in-flight beam degradation effect as well.

noise. The index i marks the i-th subscan with the same orientation of the spin axis of the satellite.

Using all $i \in [1, N]$ subscans, where N is the total number of the subscans, we can define the circular scan as some linear transformation of the d_t^i:

$$d_t = \mathsf{A}\,\mathsf{d}^i, \tag{12}$$

where $\mathsf{d}^i = \left\{d_t^i\right\}$ is the data vector, and A is the matrix of the transformation. Eq. (12) gives us the relation of a single circular scan for a fixed orientation of the spin axis. For simple summation of the subscans we obtain $d_t = (1/N)\sum_i d_t^i$. Below we shall use the circular scan as a basic element for the map-making algorithm taking into account that the variance of the instrumental noise for such a scan is expected to be $\sim N^{-1/2}$ times smaller than for each subscan, if the instrumental noise is pure white noise. For all circular scans we can define the vector of the time-ordered data $\mathsf{y} = \mathsf{M}\,\mathsf{s} + \mathsf{n}$, where M is the corresponding map-making matrix, s denotes the pixelized map and n is the noise vector [14]. It is worth noting that for the in-flight antenna beam shape reconstruction by using Jupiter's and Saturn's images, we do not need to construct whole-sky maps, because the $-40\,$dB limit of the expected Planck antenna beam shape corresponds to an angular scale $\theta_{\rm fs} \sim 5$ degrees at 30 GHz LFI, [4] and for that purpose we can use the flat-sky approximation centered around t he Jupiter's image (Fig. 4), and apply the method by [7]. Furthermore, this assumption allows us to use a linear map-making algorithm (see [14]), which is similar, for example, to the COBE pixelization scheme.[5]

The signal in each pixel of the map s is then [14]

$$\mathsf{s} = \mathsf{W}\mathsf{y}, \tag{13}$$

where W is the corresponding matrix, which depends on the scan strategy of the Planck experiment. For example, for the simplest COBE pixelization we can use $\mathsf{W} = \left[\mathsf{M}^{\rm T}\mathsf{N}^{-1}\mathsf{M}\right]^{-1}\mathsf{M}^{\rm T}\mathsf{N}^{-1}$, where $\mathsf{N} = \langle \boldsymbol{n}\boldsymbol{n}^{\rm T}\rangle$ is the noise covariance matrix. [6]

Let us go back to the single circular scan. As seen from Eq. (9) and Eq. (11), for the simple average of the subscans ($\mathsf{A} \to 1/N\sum_i$) the Jupiter's image after beam convolution in a circular scan should be

$$d_t = \frac{1}{2kN}\left[\frac{2\sinh(\eta/2)hc}{kT_{\rm CMB}\eta^2}\right]^2 \sum_i \sum_{t_i'} S_{\rm J}(\nu, t_i')B_t(\theta_i), \tag{14}$$

[4] For LFI+HFI frequency range this scale corresponds to the minimum.

[5] Note that for estimations of the in-flight beam distortions caused by $1/f$ noise, foreground contaminations and so on, [6] have to use the whole-sky map for the $1/f$ noise removal.

[6] Note that we can use any modification of pixelization without loss of information, e.g. GLESP [15, 16] or HEALPix [17].

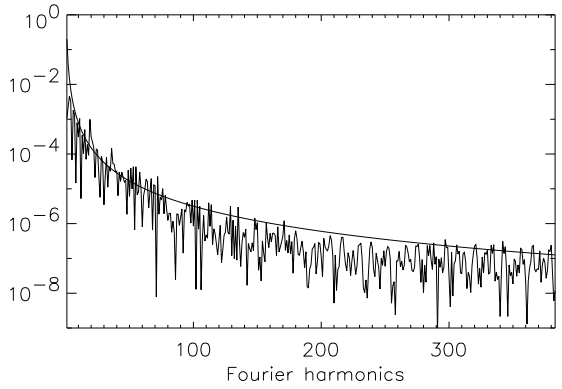

Figure 6: *The power spectrum of the flux density from Jupiter at the 13 cm wavelength, which is produced by linear interpolation in the parts of the intervals in Fig. 5 where data are not available. The fitted curve is described by a power law* $P(k) \propto k^{-2.4}$.

where $\boldsymbol{\theta}_i = \boldsymbol{r}^{'}(t_i') - \boldsymbol{r}(t_{{\rm J},i})$, $t_{{\rm J},i}$ is the Jupiter's location in the i-th subscan and B_t denotes the beam shape in each subscan. As one can see from Eq. (13) and Eq. (14), in the pixelized map the pixels containing Jupiter's image are related to the B_t and $S_{\rm J}(\nu, t_i')$ and can be denoted as follows,

$$\mathsf{s} \propto \mathsf{W}S_{\rm J}(\nu, t_i')B_t(\boldsymbol{\theta}_i). \tag{15}$$

Therefore, for the definition of the antenna beam shape in the pixel domain, we can specify some possible sources of uncertainties from Eq. (15).

Before focusing on the two categories of variabilities in beam calibration in the next two sections, we would like to briefly mention the uncertainty which is related to the location of Jupiter,

$$\boldsymbol{r}(t_{{\rm J},i}) = \overline{\boldsymbol{r}}(t_{{\rm J},i}) + \Delta\boldsymbol{r}(t_{{\rm J},i}) = \overline{\boldsymbol{r}}(t_{{\rm J},i})(1 + \delta_r), \tag{16}$$

where $\overline{\boldsymbol{r}}(t_{{\rm J},i})$ indicates the average location and $\Delta\boldsymbol{r}(t_{{\rm J},i})$ corresponds to the fluctuation of the Jupiter's location. Generally speaking, this source is related to the pointing accuracy of the Planck experiment. It is natural to assume that $\langle\Delta\boldsymbol{r}(t_{{\rm J},i})\rangle = 0$, but $\langle|\Delta\boldsymbol{r}(t_{{\rm J},i})|^2\rangle \neq 0$.

4. VARIABILITY OF THE JUPITER's FLUX ON THE BEAM CALIBRATION

The fluctuations of the Jupiter's flux can be crucial for the in-flight antenna beam shape reconstruction scheme. The temporal variations in the Jupiter's flux can be expressed as the constant flux $\overline{S}_{\rm J}(\nu)$, and a

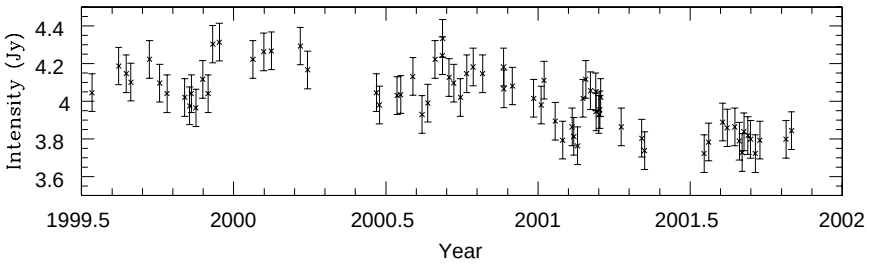

Figure 5: *Variability of the flux density of synchrotron radiation at 4.04 AU from Jupiter at 13 cm wavelength (2.3 GHz) (re-produced from [19]).*

fluctuating part $\Delta S_{\rm J}(\nu,t)$,

$$S_{\rm J}(\nu,t)=\overline{S}_{\rm J}(\nu)+\Delta S_{\rm J}(\nu,t)=\overline{S}_{\rm J}(\nu)[1+\delta_S(t)]. \quad (17)$$

Returning to Eq. (13) and Eq. (14) in order to define the beam shape properties in the pixel domain, we will assume $\langle\Delta\boldsymbol{r}(t_{{\rm J},i})\rangle=0$ (so that in Eq. (16) $\delta_r=0$). The pixelized beam can be obtained from the subscans including Jupiter's image as follows [20]:

$$B_p(\boldsymbol{\gamma})=\sum_{t\in p}\sum_i\sum_{t_i'}{\rm W}[1+\delta_S(\nu,t_i')]B_t(\boldsymbol{\theta}_i), \quad (18)$$

where γ is the angle between the position of pixel which corresponds to the Jupiter's location in a map and position of each different pixel. Possible variation of the Jupiter's flux produces an additional source of peculiarities in the pixelized beam shape definition proportional to $1+\delta_S(t)$.

4.1. Characteristic Time Scales

There are 3 characteristic time scales related to the Planck scan strategy. For each subscan of 1 r.p.m. the time scale is $T_{\rm sub}\simeq 1$ minute. The next time scale is that for a circular scan $T_{\rm cir}=60$ minutes, which is the time interval for data accumulation in one circular scan with a fixed orientation of the spin axis. In terms of order of magnitude, $T_{\rm cir}$ scale can be used for estimation of the characteristic time scale for the signal variation in one pixel around the main beam area. Another time scale is related to the scale of the far sidelobes $T_{\rm FS}\simeq\theta_{\rm FS}/1^\circ$ days, where $\theta_{\rm FS}$ is the angular measure subtended by the far sidelobes of the beam. For example, for the LFI 30 GHz channel, the threshold of -30 dB subtends the angular scale $\theta_{\rm FS}\simeq 1.5$ degrees [6] and thus $T_{\rm FS}\simeq 1.5$ days. The high-frequency fluctuations of the Jupiter's flux which corresponds to the time scales $T_{\rm sub}$, $T_{\rm cir}$ and $T_{\rm FS}$ are thus very important for the in-flight antenna beam shape reconstruction and may require more detailed investigations, for example by ground-based telescopes. These time scales also indicate that all irregularities of the Jupiter's flux for $T\geq T_{\rm FS}$ correspond to long-term variations and could mimic a beam shape degradation effect.

Unfortunately, we do not know exactly the properties of temporal variations in the Jupiter's flux in the Planck frequency range 30–857 GHz. According to the information available in the literature, the Jupiter's flux variability at a frequency of 2.3 GHz, nearest to LFI frequency range, is related to synchrotron emission from the Jupiter's magnetic belts. Fig. 5 shows the variation of the flux density of the synchrotron radiation from Jupiter at 2.3 GHz, reproduced from [19]. The interval of measurement is one day, so any fluctuation shorter than 1 day is yet to be measured. In Fig. 6 we show the power spectrum of Fig. 5, which is produced from linear interpolation in the part of the intervals where data are not available.

The temporal variation that can significantly distort the beam reconstruction for the 30 GHz channel is between 2.4 hours and 1.5 days, the Planck crossing time of Jupiter. The variation period of the Jupiter's flux shorter than 2.4 hours may be smeared out after pixelization in this channel because of the scan strategy and beam shape properties. For a variation period longer than 1.5 days, the distortion is much less.

In Fig. 7 we show simulated beam reconstructions in the 30 GHz LFI channel with possible Jupiter's flux variations. According to Eq. (17), if $\delta_S(t)$ is a random process, in the Fourier domain it can be characterized by a power spectrum. We will assume that for Jupiter atmospheric emission the power fluctuations $\delta_S(t)$ should have a form $P(\omega)\simeq a\omega^{-n}+b$, where a and b are constant. For illustration we will use the same values of a and b parameters as for the synchrotron emission discussed above (Fig. 6). The flatness of the power spectrum at large Fourier modes in Fig. 6 allows us to assume the same amplitude of the variation for different periods. Panel (a) is the recon-

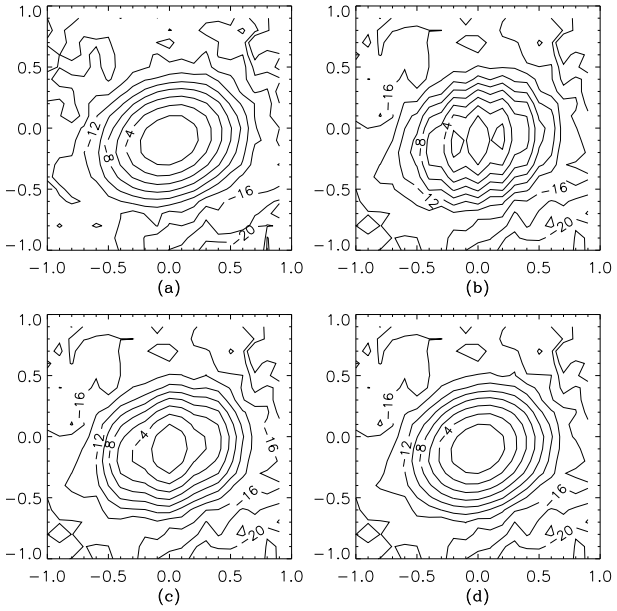

Figure 7: *Simulation of beam reconstruction with variation of Jupiter's flux. We simulate 30 GHz LFI channel (FWHM= 33′ with an ellipticity ratio =1.3) with* $\sigma_{\rm CMB}$ *and pixel noise* $\sigma_{\rm pix}$ *equal to* 3×10^{-5} *and* 8×10^{-6}*, respectively. Panel (a) is without Jupiter's flux variation, (b) with Jupiter's flux varying with a period of 4.8 hours, (c) 10 hours (the rotation period of Jupiter) and (d) 1.5 days (the Planck crossing time of Jupiter). The contour lines are annotated in dB.*

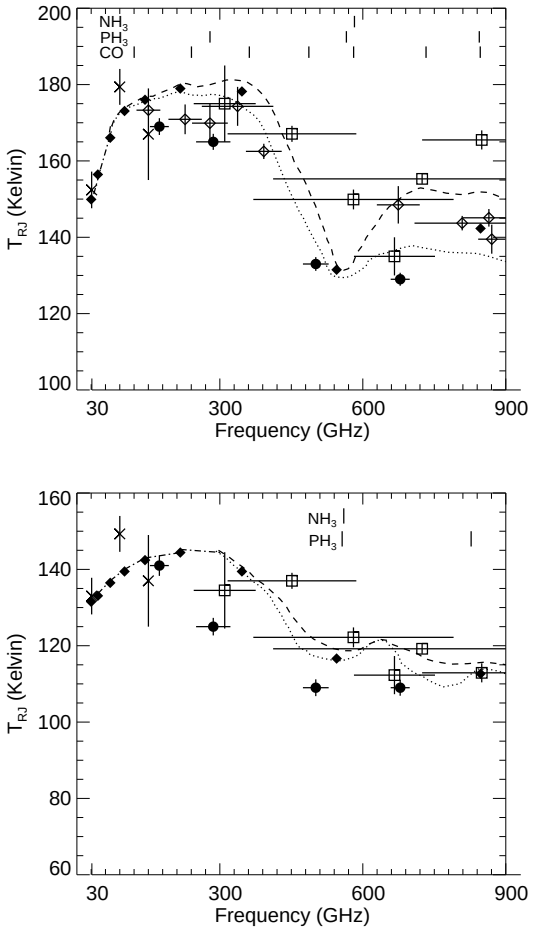

Figure 8: *The millimeter and sub-millimeter spectrum of Jupiter (top) and Saturn (bottom) (reproduced from [11]). The filled diamonds denote the fluxes calculated in this work according to the model at the 9 observing frequencies in the Planck experiment. Note that the first strong dips in the spectra coincide around Planck 545 GHz observing channel. The figure of spectrum was prepared using [11] (filled circles), [23] (diamonds), [24] (squares),[25] (crosses).*

structed image without variation in the Jupiter's flux, (b), (c) and (d) are with flux fluctuation of the variation period equal 4.8 hours, 10 hours, and 1.5 days, respectively. The period of 10 hours corresponds to that of Jupiter's rotation. The amplitude of the variations is assumed to be 20%. We can clearly see that the orientation of the main beam changes because of the fluctuation of the Jupiter's flux.

4.2. Millimeter Spectra of the Planets and Their Variations at Different Frequencies

To estimate the effects of the flux density variation of the planets, we have to look at their radio spectra. The total Jupiter's radio spectrum consists of the following two components [21]: a low radio-frequency part, which is related with the synchrotron emission from energetic electrons spiraling in the Jupiter's magnetic field, and a high radio-frequency part, which corresponds to the thermal atmospheric emission.

The synchrotron emission dominates in the frequency range $\nu \leq 10$ GHz while at $\nu \geq 30$ GHz the Jupiter's radio flux is determined by the atmospheric emission. First of all, let us describe the contribution of the synchrotron emission and its variability to the $\delta_S(t_{\rm J})$ parameter for the 30 GHz LFI channel. Recently simultaneous observations with the Cassini spacecraft, the Gallileo spacecraft and the VLA in the centimeter wavelength range have been made [18, 19]. As is shown by [18], the Jupiter's magnetosphere is strongly affected by the solar wind. When interplanetary shocks propagate from the Sun and reach Jupiter, they compress and re-configure the magnetosphere, producing a strong magnetic field and electron acceleration. The ∼10% variation with a vari-

ability of about 0.5 Jy per month of the 13 cm flux from Jupiter observed by [19], and shown in Fig. 5, may most likely be due to such an effect. This value can be used as an upper limit in our estimations. For the Planck antenna beam shape reconstruction we must, as shown earlier, know the variability of the Jupiter's flux on a time scale of $T_{\rm cir} \sim 1 \div 2$ days, to obtain the lower limit of the variation for the Planck frequency range 30–857 GHz. Obviously, the synchrotron emission is important, in principle, only for 30 GHz channel and it determines the lower limit of the Jupiter's flux variation, if the atmosphere emission does not produce any fluctuations of the flux in the 30 GHz band. We plot in Fig. 6 the power spectrum of the 13 cm synchrotron flux variability. From this spectrum we find the limit $\Delta_{\rm synch} \sim$10% per day.

If we argued that the same amplitude of the synchrotron emission also occurred at the 1 cm wavelength and used this value in our simulations, it would give the lower limit of the flux variation due to the synchrotron emission at 30 GHz of $\delta_{\rm synch} \sim (T_b^{\rm synch}/T_b)\Delta_{\rm synch} \simeq 10^{-3}$, where T_b is the brightness temperature corresponding to the total planet flux and $T_b^{\rm synch}$ that corresponding to the synchrotron emission. Thus, we can conclude that the variation of the synchrotron emission at $\nu = 30$ GHz is not important for the antenna beam shape reconstruction for the whole range of interest (≥ -60 dB). However, it is necessary to obtain additional observational data on the intrinsic atmospheric emission. [7]

Detailed studies by [11] of the millimeter and submillimeter spectra of Jupiter and Saturn have shown (see Fig. 8) that there are peculiarities in the spectra in this wavelength range. The two model spectra shown in Fig. 8 are from [23], using different physical parameters such as the size of NH_3 clumps and the particle and gas scale heights ratio. Temperatures of Jupiter and Saturn estimated at the corresponding Planck observing frequencies are shown by filled diamonds in Fig. 8. The first strong dip on both spectra almost coincides with the observing frequency 545 GHz near the 570 GHz NH_3 and PH_3 resonances. Estimated brightness temperatures with an accuracy of about 10% are given in Table 2 (see also Table 1).

Unfortunately, we do not have information about variability of the Jupiter's and Saturn's fluxes in the range 30 to 857 GHz, which determines the accuracy of the beam shape reconstruction. Some naive expectation of a possible variability in the frequency range of interest for the Planck mission could be related

[7] We would like to argue that it is natural to expect a non-zero fluctuation from the atmospheric emission. Partly our assumption is based on the millimeter and sub-millimeter spectrum of the atmospheric emission measurements at 30–857 GHz.

Table 2: *Brightness temperature T_b of Jupiter and Saturn at Planck observing frequencies with an approximately 10% accuracy*

ν (GHz)	λ (mm)	beam (arcmin)	$T_{\rm Jupiter}$ (K)	$T_{\rm Saturn}$ (K)
30	10.00	33.0	152	133
44	6.82	24.0	158	135
70	4.29	14.0	167	138
100	3.00	10/9.2	173	141
143	2.10	7.1	176	144
217	1.38	5.0	179	146
353	0.85	5.0	178	141
545	0.55	5.0	133	118
857	0.35	5.0	145	114

with the observed 20% deviations of the Jupiter's and Saturn's temperature from the pure black body law $T(\nu)$=const. For Jupiter, this 20% deviation allows us to expect that some process leading to such kind of variations can be variable in time at the same level and have the characteristic time scale close to the period of Jupiter's rotation (i.e. $\simeq$ 10 hours). This problem needs an additional and more detailed investigation by using large ground-based radio telescopes in order to measure possible variation of the Jupiter's and Saturn's fluxes in the Planck frequency range. Recent explorations of Jupiter with the radio telescope RATAN-600 have shown stability of the Jupiter's flux at the level of 0.1% at the frequency of 30 GHz for 34 days of observations [26]. Such type observations will be necessary during "in-flight" beam calibration of the Planck mission.

4.3. Expected Polarization of the Flux

One of the main goals of the Planck mission is the CMB polarization measurements. First of all, we would like to point out that a low limit of polarization of the Jupiter's flux at 30 GHz exists, which is related to synchrotron emission.

According to [27], the polarization level Π of synchrotron radiation is related to the spectral index β ($T_{\rm synch} \propto \nu^{\beta}$) as

$$\Pi = \frac{3\beta + 3}{3\beta + 1}, \qquad (19)$$

which gives $\sim$ 10÷75% for different values of Π. The total polarized flux of Jupiter and Saturn is $\sim T_{\rm planet}\Pi$. This fact creates a pre-condition to use these planets for polarized antenna beam shape calibration.

Using the value of $\beta = -1.26$ for $\nu > 13.6$ GHz for the spectral index of the Jupiter's synchrotron flux [19], one can obtain $\Pi_{\rm Jupiter}$=28%, indicating that the

polarized part of the total flux can reach around 0.3% in the 1 cm wavelength range (see Table 2).

5. EFFECTS FROM THE STRATEGY OF THE OBSERVATIONS

5.1. Variations of Planet Antenna Temperatures Versus Distance to the Planets

From the dates of crossing the scan angle by the planets, one can calculate the corresponding distance and hence the angular sizes of the planets. When the object size is sufficiently smaller than the solid angle of the beam, the antenna temperature T_a of the planet is given by

$$T_a = T_b \frac{\Omega_{\rm planet}}{\Omega_{\rm beam}}, \tag{20}$$

where T_b is the brightness temperature of the planet (Table 2), $\Omega_{\rm planet}$ is the solid angle of the planet in observation (angular size in steradian), and $\Omega_{\rm beam}$ is the solid angle of the beam calculated with a simple approximation by a Gaussian shape

$$B = \exp\left(-\frac{\theta^2}{2\sigma^2}\right), \tag{21}$$

where $\sigma \equiv \sqrt{(\sigma_-^2 + \sigma_+^2)/2} = \theta_b/2.355$ and θ_b is the FWHM of the main beam. The results of calculation of the antenna temperatures for the three frequencies 30, 100 and 545 GHz with the corresponding FWHM sizes of 33, 10 and 5 arcmin are given in Table 1.

5.2. Scan Strategy and Peculiarities of the In-flight HFI Beam Reconstruction

In this subsection we would like to focus on the discussed scan strategy of the Planck mission and its influence on the in-flight antenna beam shape reconstruction using Jupiter's and Saturn's transits. According to the Planck mission requirement, the FWHM for the 10 LFI + HFI channels is shown in Table 2. Let us concentrate on the beam shape properties above -30 dB for all LFI + HFI channels.

According to the scan strategy (see Fig.4), the orientation of the telescope spin axis during one hour (i.e. 1 r.p.m. of spin for 60 sub-scans) of observations should be stable: the orientation of the 60th sub-scan is parallel to that of the 1st sub-scan at the moment t_0 when a given circular scan starts to be measured. At the end of the 60th sub-scan, the spin axis (and the optical axis) should change its orientation by $2\farcm5$ in the ecliptic plane (re-pointing). Thus, during Jupiter's and Saturn's transits the highest resolution scale from which the images of Jupiter and Saturn can be recovered in the pixelized map is $2\farcm5$ on one side (as the sizes of both the planets are less than $1'$).

Due to the pixelization scheme, however, we will face the following two situations concerning the higher frequency channels: good and bad cases of the planet transit. The good case is where the planets are caught by the beam peak just after re-pointing and have a maximum signal on a circular scan. The probability of such a case is low. The bad case is where the planets bypass the beam maximum so that the point of maximum of the planet flux is missed by both of the neighboring circular scans. In terms of the map-making algorithm it means that the point of the maximum of the Jupiter's flux is formally shifted away from the center of the corresponding pixel and the signal in the surrounding pixels must be asymmetrical. This asymmetry can be removed using the expected $10''$ pointing accuracy if there are no temporal variations in the Jupiter's flux or no mirror degradation effect.

Thus, the map-making algorithm should reflect directly the scan strategy and the position of Jupiter and Saturn (see Fig.1 and 4). Using the -30 dB threshold, we can estimate the number of pixels, which manifests the beam shape in the map for each frequency channel. For the simple Gaussian approximation (see Eq.(21)) we get

$$N_{\rm pix}(\nu) \simeq 9 \left(\frac{\rm FWHM(\nu)}{2\farcm5}\right)^2. \tag{22}$$

As one can see from Eq. (22), $N \approx 1570$ pixels in the 30 GHz channel (FWHM $\simeq 33'$), while $N \approx 36$ pixels only for the 217 GHz (and higher) channels (FWHM $\simeq 5'$), which is obviously not enough to accurately determine these beam shape ellipticity, particularly if the ellipticity is no larger than 1.2.

6. CONCLUSIONS

In summary, regarding the issues related to using transits of planets, such as Jupiter and Saturn, as a method of calibration of the in-flight beam shape, we conclude the following:

- The high accuracy of the C_ℓ estimation by Planck will require the main beam estimation with an error of 1%, which implies that we need to measure the Jupiter's flux variation $\delta B/B = \delta_{\rm S}$ to the same level.
- For observations in the LFI frequency range, e.g. $30 \div 100$ GHz, we have a limit of possible variations of the Jupiter's flux ≤ 0.1 for the -30 dB threshold of the beam. In addition, we need to measure the variations of the Jupiter's flux by using ground-based radio telescopes.

• When observing at high frequencies (217÷857 GHz) we may have problems during observation of the planets such as missing a target due to the narrow beams.

• Practically, during the mission (≈ 15 months), we will be able to test the main beam about 3 times down to -23.5 dB by using the Jupiter's flux and 2 times by Saturn. This implies that in the case of calibrating the beam degradation effect in intervals shorter than 3 months we have to use the method by [7].

• The close (in time interval) transit of the planets will enable us to check a high–frequency component of the beam degradation.

• Neither Jupiter nor Saturn makes it possible to test the far sidelobes.

• Galactic synchrotron and dust emissions appear at a level of 0.18 mK.

• The possible degradation effect could be important at the same, as the Jupiter's flux, level of variation, $\sim 1 \div 10\%$, for the beam width.

• At low frequencies (30 GHz) of the mission, the stability of the Jupiter's flux can be monitored with the RATAN–600 radio telescope. Such a possibility was demonstrated in investigation of the planet radio flux whose stability was checked during a month at a level of 0.1% [26].

We also note that calibrations by Jupiter and Saturn, together with the method by [7], allow one to restore the antenna beam shape for pixelized beam on the ΔT map, which is different from the antenna beam shape in the frame on the focal plane. In general cases, transition from a pixelized beam to the actual beam in the focal plane frame requires a knowledge of the noise properties [7].

Acknowledgments. O.V.V. thanks the Russian Foundation for Basic Research for partial support (grant no. 05-07-90139).

References

[1] N. Mandolesi, C. R. Laurence, M. Bersanelli, et al., *Planck Low Frequency Instrument, A Proposal to ESA* (1998).

[2] J. L. Puget, G. Efstatihou, J. M. Lamarre, et al., *High Frequency Instrument for the Planck Mission, A Proposal to ESA* (1998).

[3] M. Bersanelli and J. -M. Lamarre, *Planck Systematic Effects Working Group: Objectives and Organisation*, Tech. Rep. ESA (2001).

[4] P. De Maagt, A. M. Polegre, G. Crone, *Planck – Straylight Evaluation of the Carrier Configuration*, Tech. Rep. ESA PT–TN–05967, 1/0 (1998).

[5] C. Burigana, M. Makaspina, N. Mandolesi, et al., Internal report ITESRE 198 (1997), astro-ph/9906360.

[6] C. Burigana, P. Natoli P., N. Vittorio, et al., Experim. Astron. **12**, 87 (2001).

[7] L.-Y. Chiang, P. R. Christensen, H. E. Jørgensen, et al., A&A **392**, 369 (2002).

[8] P. D. Naselsky, O. V. Verkhodanov, P. R. Christensen, and L.-Y. Chiang, *On the PLANCK in-flight antenna beam shape reconstruction using planet transit*, astro-ph/0211093v2 (2002).

[9] P. D. Naselsky, O. V. Verkhodanov, P. R. Christensen, and L.-Y. Chiang, The Planck Newsletter 8, Iss. 5, ESA, (2003), (www.rssd.esa.int/SA/PLANCK/docs/Newsletters/PlanckNewsletter5.pdf).

[10] E. C. Downey, XEphem Version 3.5.2, `http://www.clearskyinstitute.com/xephem/xephem.html` (2002).

[11] A. B. Goldin, M. S. Kowitt, E. S. Cheng, et al., Astrophys. J. **488**, L161 (1997).

[12] L.-Y. Chiang, H. E. Jørgensen, I. P. Naselsky, et al., MNRAS **335**, 1054 (2002).

[13] N. Mandolesi, M. Bersanelli, C. Burigana, and F. Villa, Astro. Lett. Comm. **37**, 151 (2000).

[14] M. Tegmark, Astrophys. J. **470**, 81 (1996).

[15] A. G. Doroshkevich, P. D. Naselsky, O. V. Verkhodanov, et al., Int. J. Mod. Phys. D. **14**, 275 (2005), astro-ph/0305537.

[16] O. V. Verkhodanov, A. G. Doroshkevich, P. D. Naselsky, et al., Bull. Spec. Astrophys. Obs. **58**, 40 (2005).

[17] K. M. Górski, E. Hivon, A. J. Banday, et al., Astrophys. J. **622**, 759 (2005), astro-ph/0409513.

[18] D. A. Gurnett, W. S. Kurth, G. B. Hospodarsky, et al., Nature **415**, 985 (2002).

[19] S. J. Bolton, M. Janssen, R. Thorne, et al., Nature **415**, 987 (2002).

[20] J. H. P. Wu, A. Babbi, J. Borrill, et al., ApJS **132**, 1 (2001).

[21] B. F. Burke and K. L. Franklin, J. Geophys. Res. **60**, 213 (1955).

[22] *The Scientific Programme of Planck*, astro-ph/0604069, (http://www.rssd.esa.int/Planck).

[23] M. J. Griffin, P. A. R. Ade, G. S. Orton, et al., Icarus **65**, 244 (1986).

[24] R. H. Hildebrand, R. F. Loewenstein, D. A. Harper, et al., Icarus **64**, 64 (1981).

[25] B. L. Ulich, AJ **86**, 1619 (1981).

[26] Yu. N. Parijskij, N. N. Bursov, A. B. Berlin, et al., Astron. Lett. **30**, 276 (2004).

[27] S. Cortiglioni and T. A. T. Spoelstra, A&A **302**, 1 (1995).